Chemical Engineering Science 65 (2010) 4285–4292

Contents lists available at ScienceDirect

Chemical Engineering Science

journal homepage: www.elsevier.com/locate/ces

A new method for *in situ* concentration measurements in packed-column transport experiments

J. Matthew Thomas [a,*], Constantinos V. Chrysikopoulos [b]

[a] Department of Civil and Environmental Engineering, University of California, Irvine, CA 92697, USA
[b] Department of Civil Engineering, University of Patras, Patras 26500, Greece

ARTICLE INFO

Article history:
Received 25 June 2009
Received in revised form
30 March 2010
Accepted 16 April 2010
Available online 20 April 2010

Keywords:
Porous media
Sintering
Visualization
Transport processes
Packed-column experiments
Fluorescence

ABSTRACT

A new method for accurately measuring *in situ* conservative tracer and colloid concentrations in packed columns was developed. The method consists of fabricating clear sintered glass-bead-packed columns, taking digital photographs of the column under an ultraviolet light source, and determining concentrations by measurement of the fluorescence intensity of the tracer or colloids in the photographs. The sintering process prevents changes in the geometry of the porous medium making it particularly useful for contaminant transport experiments in packed columns in the presence of seismic or acoustic wave vibrations. Because fluorescence is measured, the method of quantification is limited to fluorescent tracers and fluorescent colloidal suspensions. The method is shown to be within 3% of the accuracy of traditional effluent sampling and analysis procedures and allows for quick and accurate *in situ* measurement of dissolved or suspended tracer concentrations at multiple times. However, the method is not useful for decaying chemical species unless the decay rate constant is known in advance, because the intensity curves at all times must be scaled to the known injected mass to yield concentrations.

1. Introduction

Ever after the famous packed-column experiments conducted by Henry Darcy (1856), numerous studies have employed packed columns to investigate the characterization of hydrological parameters such as porosity, dispersion, and dispersivity of natural soils (Liu et al., 1992); virus fate and transport in the subsurface environment including attachment, detachment, and inactivation (Anders and Chrysikopoulos, 2005, 2009; Jin et al., 2000; Keller et al., 2004; Masciopinto et al., 2008; Zhuang and Jin, 2003); bacteria transport and deposition kinetics in porous media (Chrysikopoulos et al., 2010; Olson et al., 2004; Rockhold et al., 2005; Sherwood et al., 2003; Tufenkji, 2007; Wang and Ford, 2009); transport and deposition of protozoan oocysts (Harter et al., 2000); attachment, detachment, straining, blocking, ripening, and decay, of colloids under various soil, solution chemistry, and saturation conditions (Bradford et al., 2004; Shang et al., 2008); nanoparticle interactions with contaminants for environmental remediation (Li et al., 2008; Zhang, 2003); single and multicomponent reactive chemical transport (Dai and Samper, 2004); cosolvent–water displacement (Harmon et al., 1999); application and effects of various waves (e.g., acoustic, seismic, and shock waves) on solutes, colloids, and NAPL dissolution, and mobilization (Beresnev et al., 2005; Chrysikopoulos and Vogler, 2004; Gross et al., 2003; Kumar et al., 2007; Li et al., 2005; Roberts, 2005; Roberts et al., 2001; Thomas and Chrysikopoulos, 2007; Vogler and Chrysikopoulos, 2002, 2004); and validation of hydrogeochemical models of saltwater intrusion (Gomis-Yagües et al., 1997). The staggering diversity of applications and number of packed-column experiments in the literature demonstrates their critical role as a tool for enhancing our understanding of the physical, chemical, and hydrodynamic processes governing the transport and remediation of contaminants in groundwater aquifers.

Depending upon the application, columns may be packed with natural soils and sediments or intact soil or rock cores from a field site of interest (DeNovio et al., 2004), or with natural or synthetic porous media such as glass beads, quartz sand, sieved-sand fractions, or crushed rock (Harmon et al., 1999). In a typical transport experiment water flows through the packed column in one direction, a chemical, tracer, or colloidal suspension is injected into the influent, and effluent samples are collected at various times and analyzed to determine the corresponding concentrations. The method of analysis depends on the type of chemical, tracer, or colloids used. In addition, depending on both the desired application and the method of quantification, the columns themselves can be made of various materials. Column parameters (e.g., porosity and dispersivity), chemical reactions or

* Corresponding author. Tel.: +1 19492323923; fax: +1 19498243672.
E-mail address: jmthomas@uci.edu (J. Matthew Thomas).

0009-2509/$ - see front matter © 2010 Elsevier Ltd. All rights reserved.
doi:10.1016/j.ces.2010.04.014

dissolution, and hydrodynamic parameters (e.g., interstitial velocity and dispersion) can be determined by fitting an analytical solution to effluent concentrations. Despite their efficacy for increasing our understanding of various physicochemical and biological processes, there are a few inherent weaknesses of these types of packed-column experiments.

First, in conventional experiments involving columns packed with a loose granular porous medium, such as sand or glass beads, the flow of water alone is often enough to cause settling of the medium over time. Rapid flushing or backflushing between experiments may quicken the settling process. In experiments involving seismic or acoustic wave propagation along a column, the process of settling or compaction is accelerated and exacerbated. In experiments where the length of the column is oriented horizontally the settling of the porous medium causes a preferential flow path to develop along the top inner wall of the column. This scenario is essentially the same as a dual permeability porous medium or the presence of a fracture within a porous medium that gives rise to two separate flow velocities: a slower interstitial velocity within the bead pack and a faster fracture (preferential) velocity within the macroscopic void space or fracture. Consequently, if the settling of the medium is not detected (e.g., in columns that are not made of a transparent material) and accounted for, breakthrough curves of tracers will be inconsistent and inaccurate because the tracer may become entrained in the region of the slower velocity, faster velocity, or partially in both. Furthermore, the different velocities will likely be impossible to determine independently because the column porosity may continuously change over the duration of an experiment. An example can be seen in Fig. 1, which shows the experimentally determined average velocity of several short-duration tracer pulses injected into a packed column subjected to acoustic wave vibration over time. The first two pulses (prior to settling) had the same average velocity. As the experiment progressed, settling occurred, and subsequent velocities were unpredictable. The velocities greater than the initial average velocity (i.e., above dashed line) were due to the tracer being partially or fully entrained in the region of faster moving velocity while the velocities smaller than the initial value were due to entrainment in the region of slower velocity. It must be noted that the column in this experiment was packed with glass beads using commonly used and approved methods. Clearly, a rigid system of interconnected grains that cannot permanently deform nor settle would be advantageous for packed-column experiments, especially for those involving seismic or acoustic waves.

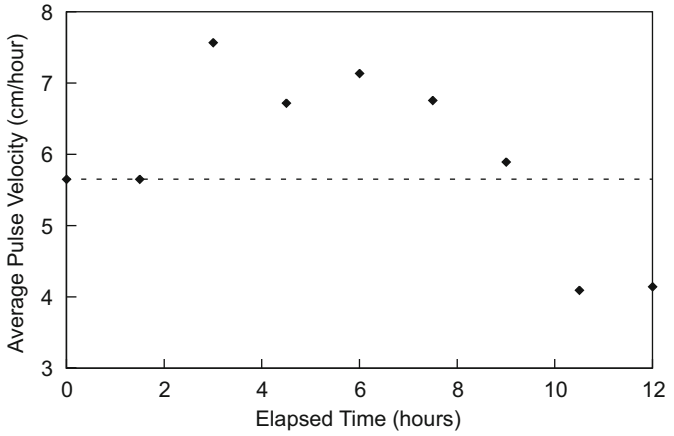

Fig. 1. Experimentally determined average velocity (solid diamonds) of nine short-duration tracer pulses injected into a packed column subjected to acoustic wave vibration over time. The dashed line represents the initial average velocity with no acoustics.

Second, concentration measurements of chemicals, tracers, or colloidal suspensions as they flow through a column (*in situ*) cannot be determined. Therefore, the effect of the spatial and temporal changes in hydrochemical and hydrodynamic conditions on contaminant transport cannot be distinguished because concentrations obtained from column effluents represent some average behavior and the processes that control contaminant transport in the column are obscured (Baumann and Werth, 2004). We note that a number of experiments utilizing fluorescence to obtain *in situ* velocity and concentration measurements of small particles have been performed (Northrup et al., 1993; Peurrung et al., 1995; Rashidi et al., 1996). However, each of these focused on the micro-scale and then volume-averaged those results to obtain macroscopic concentrations of particles rather than making macroscopic measurements. Additionally, these studies utilized indexed matched silicon oils to saturate the porous medium, rather than water, and may not be indicative of groundwater flow. More recently, other visualization methods have been developed utilizing fluorescence with a water-saturated porous medium (Yoon et al., 2006). Again the micro-scale concentrations were volume-averaged to obtain macroscopic concentrations and packed columns were not used. Consequently, a new method capable of detecting *in situ* concentrations in a water-saturated packed column at multiple times (snapshots) is desirable.

Finally, traditional procedures involving effluent sample collection, followed by chemical analysis is labor intensive and time consuming. For example, in one set of experiments involving a fluorescent tracer and suspensions of fluorescent colloids, standard effluent fluorescence analysis required a minimum of 30–40 samples collected every 2 min, preparation of samples by dilution, and preparation of standard solutions of known concentrations, followed by fluorescence analysis (Thomas and Chrysikopoulos, 2007). Certainly, a method for quantification that can be performed quickly to yield the *in situ* concentrations would be beneficial.

The present work is an attempt to overcome the aforementioned weaknesses. The newly developed method is aiming to construct a rigid porous medium that would not deform permanently under the forces of flow nor acoustic or seismic vibration, to allow for visualization of the medium and make *in situ* concentration determinations at multiple times while experiments are in progress, and to make the concentration determinations less time consuming.

2. Methodology

The new method consists of fabricating optically clear sintered-glass-bead-packed columns, taking digital photographs of the tracer as it flows through the column under an ultraviolet light source, determining concentrations by measurement of the intensity of fluorescence of the tracer in photographs using the MATLAB® Image Processing Toolbox™, and calibrating with traditional effluent sample analysis to ensure the accuracy of the results obtained.

2.1. Fabrication of sintered-glass-bead column

One way to create a porous medium that will not deform nor settle is to sinter the glass beads in place within the column. Sintering is the process of heating glass beads beyond their transition temperature, the temperature at which glass begins to deform, which causes separate beads of glass to flow together and fuse at points of contact (viscous flow sintering or first stage sintering). The glass must then be cooled rapidly below the

transition temperature to prevent further sintering. The sintering process has some inherent difficulties. Glass is an amorphous solid produced by heating normally crystalline compounds to their melting point to produce a homogeneous mixture, then cooling the mixture rapidly so that re-crystallization cannot occur. Therefore, when glass is heated to the point that it begins to flow, molecules on the surface of the glass tend to crystallize. The crystallized surfaces are not able to flow together and therefore act as a barrier to further sintering, preventing the formation of the desired rigid medium. Furthermore, surface crystals scatter the light shining through them, which is undesirable because this method relies on measuring the intensity of fluorescent light emitted from the tracer, which must travel through the sintered medium. We note that Plona (1980) had produced a sintered glass-bead porous medium but that it was not within a column nor was it used for transport experiments.

The sintering temperature can vary the relative kinetics of sintering and crystallization (Prado et al., 2003). The literature suggests that high temperatures favor sintering over crystallization (Barg et al., 2008). However, at high temperatures sintering occurs rapidly, cooling the glass below the transition temperature takes longer, and consequently, it is difficult to consistently reproduce the same degree of sintering. The temperature ranges considered in the literature are well above the transition temperature of glass. However, it is commonly known to glassblowers that fusing of glass can be accomplished at lower temperatures near the transition temperature, without producing significant crystallization. There is very little literature covering the lower range of temperatures just above the transition temperature. Our aim was to determine if it was possible to produce significant sintering in this lower temperature range just above the transition temperature of the glass beads, without producing significant surface crystallization. Thus, sintering requires a furnace whose temperature can be precisely controlled to quickly heat the glass to the desired temperature and then rapidly cool the glass so that crystallization is minimized. Our preliminary sintering tests were performed with 1 mm soda-lime glass beads at temperatures just above the transition temperature (approximately 650 °C), and showed that significant sintering was accomplished with little crystallization. Fig. 2 shows the selected temporal temperature program input to the Isotemp Programmable Muffle Furnace (10-650-126; Fisher Scientific, Pennsylvania), which was developed from various preliminary glass-sintering tests. Similar testing should be performed prior to fabricating columns with different bead sizes.

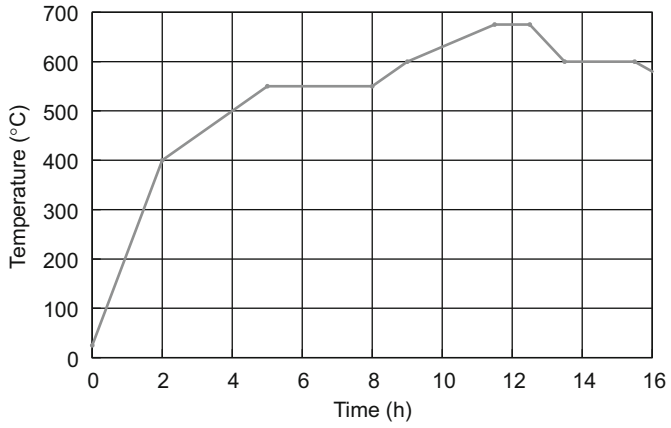

Fig. 2. Furnace temperature temporal variation program determined from preliminary sintering tests with 1 mm soda-lime glass beads without substantial crystallization.

An injection port was fitted to the middle of a 30-cm-long borosilicate glass chromatography column (Kimble Kontes, New Jersey) with a 2.5 cm inner diameter (see Fig. 3). To prevent the column from deforming during the sintering process, a mold was created by cutting a stainless steel tube in half, lengthwise. Stainless steel expands but does not deform at the temperatures used to sinter the glass. The column was enclosed between the two halves of the steel tube. The tube was fit into a vertical cylindrical groove that was ground into red clay bricks. The vertical orientation was necessary to prevent the beads from slumping and pulling away from the inner column wall, as would happen if the column were lying flat. Steel wire was wrapped through holes that were drilled in the brick and around the steel tube to hold the column in place within it. Circular pieces of fine-mesh stainless steel screen were cut to a diameter slightly smaller than the inner diameter of the column to temporarily retain the beads within the column during sintering. A stainless steel spacer was used to maintain the bottom screen at the proper location in the column so that the column end caps would still fit after the completion of sintering. The vertically oriented column was then filled with soda-lime glass beads of 1 mm diameter (Fisher Scientific, New Jersey). Another screen was placed on top of the glass beads at the other end of the column and a small stainless steel weight was added. This weight applied just enough force as the beads began to slump during sintering to close the gaps created and ensure a more uniform porosity in the longitudinal direction. Fig. 3 is a photograph of the column retained in the brick, and the steel tube mold assembly. Finally, the entire mold and column filled with glass beads were placed in the Isotemp furnace and heated according to the temperature program presented in Fig. 2.

The temporary screens and spacers were removed and the column was capped with polytetrafluoroethylene (PTFE) column end fittings on both the influent and effluent ends. The end fittings were secured by plastic screw caps that screw into threads molded in the ends of the glass column. The column was connected to a dual-syringe infusion pump (KDS200; KD Scientific, Massachusetts) and a tactile sound transducer acoustic

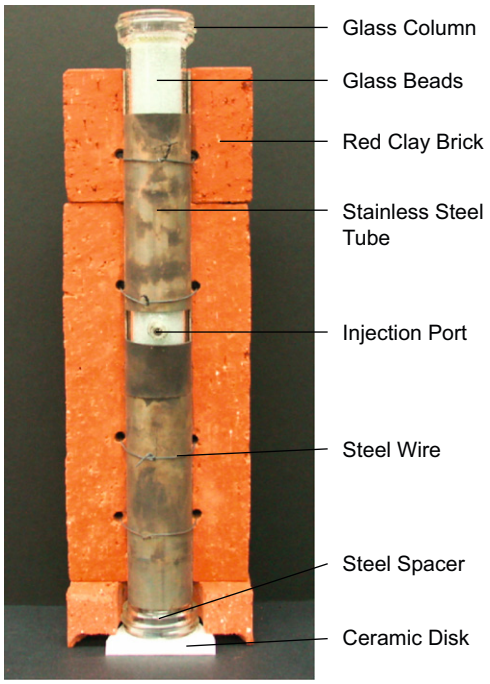

Fig. 3. Apparatus used for sintering the experimental column.

source (TST429-Platinum; Clark Synthesis, Colorado) and was filled with degassed purified water and purged of any entrapped air. Finally, small marks were etched onto the glass column for accurate scaling of the photographs. One mark was etched at the point of injection and indicates the x-coordinate origin, while the other mark was etched exactly 14 cm down the column in the direction of flow. All experiments were performed with a constant flow of purified water at a rate of 0.2 mL/min through the column.

2.2. Photographic methods

An enclosure was built around the column to shut out ambient light. The enclosure was equipped with a fluorescent ultraviolet (UV) light source (GA9718P-T8-BK-I; Good Earth Lighting, Illinois) and a 35 mm digital camera (Dimage A1; Konica Minolta, New Jersey) with a remote exposure cord (see Fig. 4). The lens was equipped with a UV filter to ensure that none of the UV source light reached the CCD. Any digital camera will work as long as it has a color mode that employs the sRGB color space, and the ability to both automatically and manually set aperture, shutter speed, camera sensitivity (ISO), and focus. The ability of the camera to take a series of photographs on a set time interval is convenient but not essential. For any long duration experiments (e.g., no flow/diffusion) heat buildup within the enclosure even from a fluorescent UV source can cause circulation flow in the column. In order to prevent this, the source was connected to a programmable outlet timer (SE-11P; UPM, Calgary, Alberta, Canada) that was set to turn on for 2 min before a photograph was taken and shut off less than 1 min after. For shorter duration experiments it was determined that heat build up did not cause circulation.

Prior to running experiments for a particular tracer some preliminary photographic steps were necessary. The camera was set to the natural color mode (sRGB color space). The tracer of the same concentration to be used in the experiments was injected into the column and a photograph was taken using the auto exposure-mode setting of the camera. The maximum intensity of light emitted from the tracer and recorded for each pixel is greatest in this first photograph, where the tracer is most concentrated. Therefore, this allowed the camera to determine the proper aperture, shutter speed, and sensitivity (ISO) necessary so as not to exceed the maximum recordable intensity value, because all subsequent photographs have lower recorded intensity for each pixel as the tracer disperses. The camera was then set to the manual mode with the aperture, shutter speed, and sensitivity determined from the first photograph. The focus was also manually set so that it did not change throughout the experiment. These steps were necessary to ensure that the intensities in subsequent photographs could be directly compared to one another without any scaling and that the maximum recordable intensity value was never exceeded.

A photograph was taken with the UV source on and with no tracer injected in the column (background image). Next, the tracer was injected into the column with flow conditions determined for the experiment. Digital photographs were taken at intervals determined by the required flow rate and the desired number of concentration curves.

2.3. Image processing

An sRGB image is stored as a three-dimensional (3-D) array consisting of three 2-D arrays of pixel intensities, one for red, one for green, and one for blue. Each 2-D array has x and y dimensions corresponding to the rows and columns of pixels in the image with an intensity value on a scale from 0 to 255 stored in each location. These images can be easily manipulated with matrix operations, and light intensities can be converted to concentrations. The images of the tracer in the column were processed using the MATLAB® Image Processing Toolbox™ in a manner similar to Bouhairie (1998). In the subsequent paragraphs all of the functions employed refer to the MATLAB® Image Processing Toolbox™ terminology (MathWorks, Inc., 2008).

The total number of pixels (image size) and the file type and compression rate (image quality) of the image were set in the camera, while the actual area covered by the pixels changed as the camera was zoomed in or out. For this reason and because we are interested in measuring the tracer as it moves through the column, the first step was to map the pixels in the images to actual locations along the length of the column (i.e., in the x-direction). This was accomplished by using the 'imtool' function to count the number of pixels between the markings etched into the column. In order to obtain the actual length per pixel, the 14-cm distance between the two markings on the column was divided by the number of pixels. Then the injection location marking was fixed as $x=0$, and the locations of the center points of each of the pixels were fixed to actual spatial locations in the x-direction.

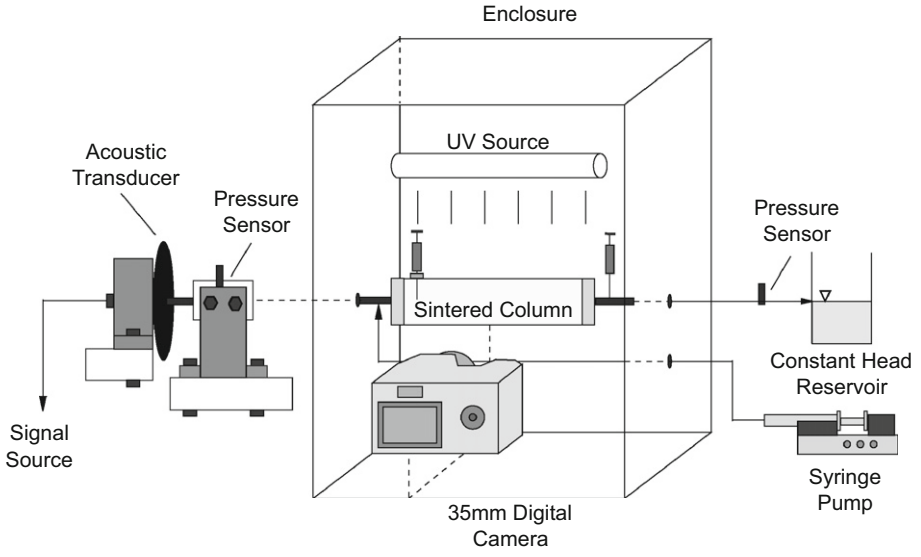

Fig. 4. Experimental set-up.

Next, the background image taken at the beginning of the experiment was subtracted from the subsequent tracer images using the 'imsubtract' function. The resultant images consist only of the fluorescent light emitted from the tracer as it moved through the column. However, the light emitted from the tracer was scattered as it traveled through the glass-bead pack and the column walls causing the tracer to appear more longitudinally dispersed than it actually is. This 'optical dispersion' was corrected in the calibration step.

The 'imtool' function was used to select rows and columns of pixels along the column's boundaries to act as cropping limits. Then, all but the column area was cropped from the image and the resultant RGB image was separated into its red, green, and blue component images. The component image with the highest intensity for a particular tracer was selected and further processed to determine *in situ* concentrations. The other two component images are not needed. Fig. 5 shows cropped images from an experiment with uranine tracer injection into the packed column. Note that each image in Fig. 5 was cropped and mapped to the true spatial location. The intensity values for the pixels in vertical columns were added and then divided by the total number of pixels in the column to obtain the column-averaged intensity. To reduce the total number of column-averaged intensity values and produce a smooth curve, a bin size of 50 columns was chosen and the column-averaged intensity values in each bin were averaged and assigned to the location of the center of the bin.

Finally, there was a slight increase in the overall brightness of all the background-image-subtracted tracer images compared to the background image because the light emitted from the tracer is reflected inside the enclosure. This shows up as a uniform baseline intensity that is greater than zero. That is, a plot of the intensity curve in the x-direction will not approach zero with distance from the tracer, but rather a baseline value of the ambient intensity inside the enclosure. A reasonable baseline intensity estimate was selected by visual inspection and subtracted from the bin-averaged intensities. As illustrated in Fig. 6, what remains is a curve of intensity values at fixed locations in the x-direction along the column that must be calibrated by scaling to the total injected mass and by correcting for optical dispersion to yield the actual tracer concentrations along the column. Pixel intensity values range from 0 to 255 for 8-bit RGB images.

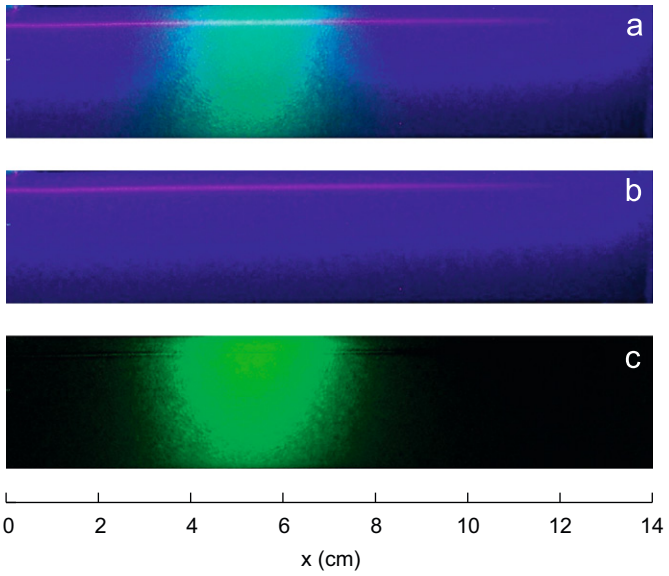

Fig. 5. Cropped images from an experiment with uranine tracer injection into the packed column showing (a) the initial RGB image, (b) the background image before the tracer was injected, and (c) the image of intensity of green light after the background image was subtracted.

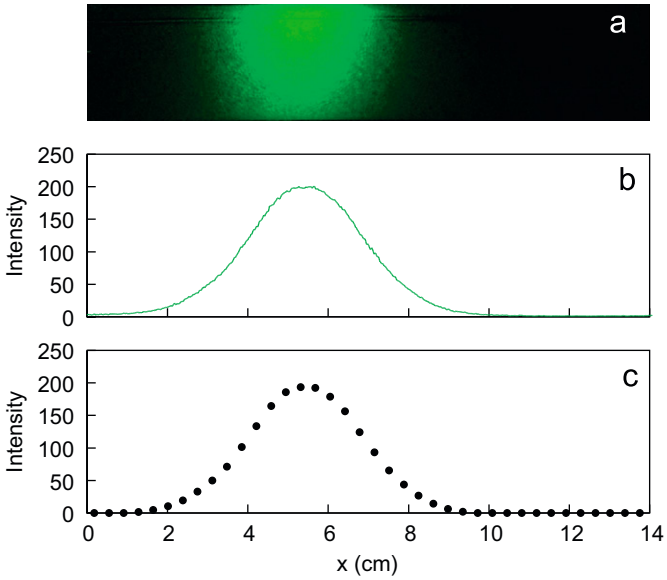

Fig. 6. Image of (a) the green light intensity, (b) the column-averaged pixel intensity curve (green line), and (c) the bin-averaged pixel intensity curve (solid circles) after the baseline was subtracted.

3. Calibration

There are two additional obstacles to creating accurate concentration curves from the intensity curves. First, the total intensity of the light (area under the intensity curve) emitted from the tracer that reaches the camera increases in magnitude at early times, so it is not possible to directly correlate the magnitude of intensity at a single pixel location to concentration. Therefore, the total intensity must be scaled to the known injected mass in order to yield the proper tracer concentrations along the column at all times. Second, there is the previously mentioned problem of optical dispersion, which was corrected by performing a calibration experiment with traditional effluent sampling and analysis.

3.1. Mass scaling

The tracer was injected into the center of the cross-section of the column. Fig. 7(a) shows that as the tracer was carried along by the flow (i.e., from t_1 to t_2 to t_3), it spread in the direction of flow along the length of the column and outward (transverse) toward the walls of the column. The intensity of fluorescent light emitted from the tracer was directly proportional to the concentration of the tracer in the column. However, not all the light emitted by the tracer reached the camera. The fluorescent light emitted from the tracer in the column had to pass through the sintered-glass beads and the column wall before exiting the column and reaching the camera. Thus at early times when the tracer is concentrated near the center of the circular cross-section, the light emitted from it must pass through more sintered-glass beads than at later times when the tracer has spread closer to the column walls (that is, in Fig. 7(a) $d_1 > d_2 > d_3$, where d is the distance between the tracer plume and the column wall). Clearly, the CCD in the camera only registered and recorded the intensity of the fluorescent light emitted from the tracer that actually reached the camera.

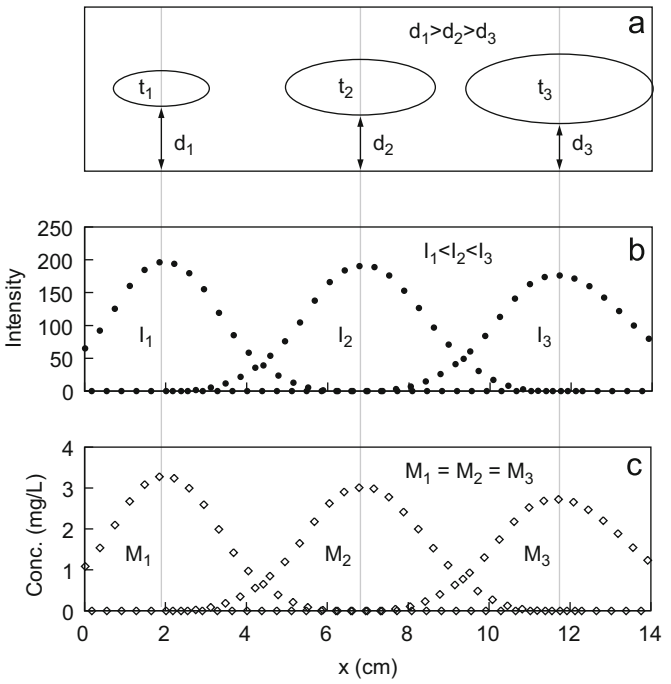

Fig. 7. Schematic illustration of: (a) the migrating tracer plume within the column at three different times, $t_1 < t_2 < t_3$, indicating that due to spreading the plume distance from the column wall decreases with time, $d_1 > d_2 > d_3$, (b) the corresponding bin-averaged intensity curves with total intensity of the emitted light that increases as the plume spreads with increasing time, $I_1 < I_2 < I_3$, and (c) the corrected concentration curves indicating that the total mass of the injected conservative tracer remains constant with time, $M_1 = M_2 = M_3$.

Scattering of the light occurred, due primarily to refraction, as it passed into and out of individual glass-bead surfaces and water-saturated pore spaces. Thus the intensity of light that actually reached the camera, while directly proportional to tracer concentration, was inversely proportional to the number of beads it had to pass through. The combined effect of dispersion and light scattering was an increase of the total intensity of light emitted from the tracer that was recorded in each image. This is difficult to see in Fig. 7(b) because the increase is only slight, nevertheless, the total area under the bin-averaged intensity curve (solid circles) increases (that is, $I_1 < I_2 < I_3$, where I is the total intensity). Because the total intensity of the light emitted by the tracer that reaches the camera increases with time during an experiment, it was not possible to produce standards of known concentration to directly relate the recorded intensity to tracer concentration in the column. However, the total mass injected into the column does not change, so the total intensity was scaled to the known injected mass to yield concentration curves. Thus the concentration is averaged over each transverse (perpendicular to the flow) slice of the column. It should be noted that this is analogous to the flux concentration measured at the column exit (Kreft and Zuber, 1986; Parker and van Genuchten, 1984). This produced a concentration curve that yielded the proper total injected mass as can be seen in Fig. 7(c) (open diamonds), where M is the total tracer mass injected and consequently, $M_1 = M_2 = M_3$, but was more longitudinally dispersed than the actual tracer in the column due to optical dispersion. Once the mass scaling was performed and concentration curves were obtained, the dispersion coefficient was corrected for optical dispersion.

3.2. Optical dispersion correction

The simple refraction of light through many beads caused a significant amount of scattering (optical dispersion), making the tracer to appear more dispersed than it actually was. This added dispersion was corrected by running a calibration experiment using the experimental methods described above, taking photographs every 2 min while the tracer remained in the column, then collecting the effluent at 2-min intervals for traditional fluorescence analysis with a Fluoromax®-4 spectrofluorometer (Horiba Jobin Yvon, New Jersey). The sample concentrations were quantified by comparing to a set of standards with known concentration. A previously derived analytical solution (of the form $C(t,x)$) to the partial differential equation that describes the transport of colloidal particles in one-dimensional homogeneous, water-saturated porous media accounting for adsorption and inactivation (Thomas and Chrysikopoulos, 2007) was fitted to the effluent concentration curve (i.e., at a fixed location, x) in order to determine the actual hydrodynamic dispersion coefficient. The analytical solution was fitted to the concentration curves obtained from each photograph (i.e., at a fixed time, t) after mass scaling, which yielded a constant dispersion coefficient that was greater than that obtained through effluent sampling, due to optical dispersion. Fig. 8 depicts the methodology just described. Because the fitted dispersion coefficient was constant, a dispersion correction factor, $c_f = D_{\text{Effluent}}/D_{\text{Mass-scaled}}$, where D_{Effluent} and $D_{\text{Mass-scaled}}$ are the fitted dispersion coefficients for the effluent breakthrough curve and the mass-scaled intensity (concentration) curve, respectively, was calculated each time. To correct for

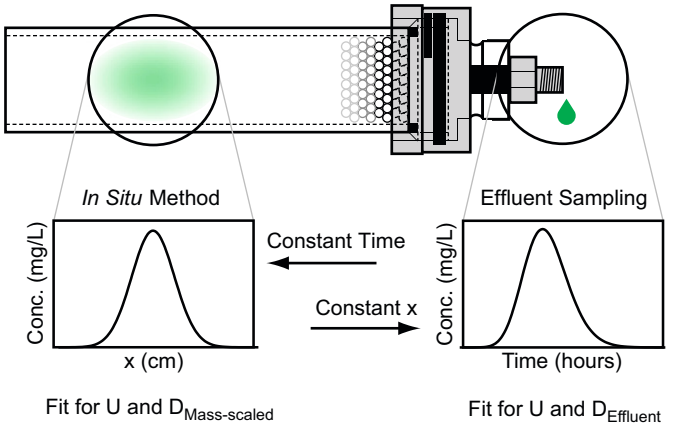

Fig. 8. Schematic illustration of the mass-scaled *in situ* intensity (i.e., concentration) curve at a fixed time and the effluent concentration curve at a fixed location that can be fitted by a previously developed analytical solution to obtain the desired coefficients $D_{\text{Mass-scaled}}$ and D_{Effluent}.

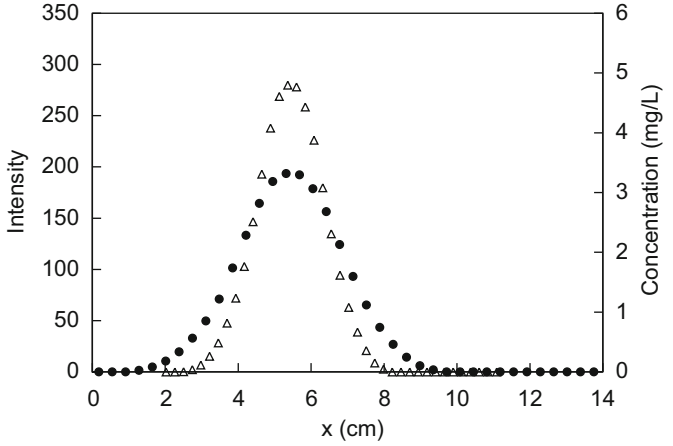

Fig. 9. A bin-averaged pixel intensity snapshot (solid circles) and the corresponding calibrated concentration snapshot (open triangles).

optical dispersion in subsequent experiments, this correction factor was multiplied by the fitted dispersion coefficient of the mass-scaled intensity concentration curves. The critical assumption is that the ratio c_f is the same for other experiments with different dispersion coefficients. Therefore, this produced a final concentration curve for all times that was practically identical to the one obtained from directly sampling and analyzing the column effluent. Fig. 9 shows the same intensity curve (solid circles) as in Fig. 6 along with the corresponding concentration curve after mass scaling and optical dispersion correction (open triangles). Because optical dispersion is a function of the structure of the sintered column as well as the fluorescent properties of the specific tracer used, a separate calibration should be performed for each column and each tracer.

4. Verification

An experiment with acoustic vibration was performed to verify that the method was accurately measuring *in situ* tracer concentrations. First, the uniformity of the column porosity was verified. An injection of 40 μL of Uranine at a concentration of 500 mg/L was made into the column with a background flow rate of 0.2 mL/min and no acoustic source pressure (base case). It should be noted that fluorescent dyes such as Uranine are organic substances whose molecules are capable of converting excitation energy caused by light into fluorescence, and they are commonly used in subsurface fluid tracing because they are inexpensive, relatively non-toxic and very easy to detect by spectrofluorometry (Chrysikopoulos, 1993). Photographs were taken at 2-min intervals. The interstitial velocity at any location x is given by $U_x = Q/A\theta_x$, where Q is the volumetric flow rate, A is the cross-sectional area of the column, and θ_x is the porosity at location x in the longitudinal direction. Therefore, if θ_x changes in the x-direction, U_x will also change, because Q and A are constant. The first moment, m_1, of the intensity curve at each 2-min interval was calculated and plotted against time, t, as shown in Fig. 10. The first moment represents the location of the center of mass as it travels in the column. For a conservative non-sorbing tracer, the center of mass travels with the interstitial velocity. A line was fitted to the plot of m_1 versus t and the R^2 statistic was calculated as 0.9997. The slope of the line given by m_1 versus t is the interstitial velocity, U_x. The R^2 statistic indicates that interstitial velocity and therefore the porosity did not significantly change along the x-coordinate. Thus, the process has produced a column with uniform porosity.

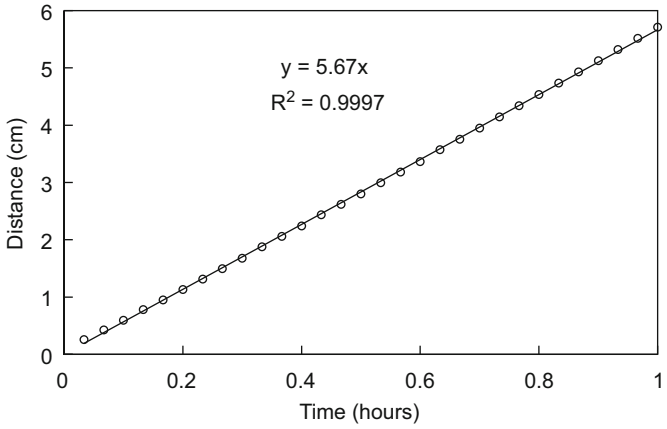

Fig. 10. The distance from the injection point to the center of mass, m_1, of the injected tracer versus time (open circles) and fitted linear trend line (solid line). The slope of the solid line represents the interstitial velocity, $U = 5.67$ cm/h, and the practically perfect R^2 statistic indicates that the interstitial velocity and therefore the porosity do not change along the length of the column.

Next, an injection of 40 μL of Uranine at a concentration of 500 mg/L was made into the column with a background flow rate of 0.2 mL/min, the acoustic source frequency set to 70 Hz, influent acoustic pressure amplitude set to 23.0 kPa, and photographs were taken every 2 min. The intensity curves obtained from each photograph were scaled to the known injected mass to obtain tracer concentration curves. The analytical solution derived by Thomas and Chrysikopoulos (2007) was fitted to the tracer concentration curves to obtain the interstitial velocity, U_x, and the hydrodynamic dispersion coefficient, $D_{\text{Mass-scaled}}$, which was corrected by multiplication with the dispersion correction factor, c_f, obtained from the calibration step, to yield the true *in situ* hydrodynamic dispersion, D, which is equivalent to D_{Effluent}. Finally, the effluent was collected and analyzed with a Fluoromax®-4 spectrofluorometer (Horiba Jobin Yvon, New Jersey), and the analytical solution was fitted to the measured tracer concentration curve (i.e., breakthrough curve). Both the interstitial velocity and hydrodynamic dispersion determined by our method were found to be within 3% of those determined by direct effluent sampling and analysis.

5. Conclusions

The method developed produces a rigid porous medium that produces consistent and reproducible results. Preferential flow paths are prevented making it particularly useful for seismic or acoustic vibration packed-column experiments. The method was shown to be as accurate as standard effluent sampling and allows for accurate *in situ* measurement of tracer concentrations at multiple times. Standard effluent fluorescence analysis requires a minimum of 30–40 samples at 2 min each, preparation of samples including dilutions, and standard solution preparation and analysis. After calibration, the same analysis can be accomplished with this method in a few seconds. In addition, the method also allows the capture of concentration data at multiple time steps. With this method it is possible to perform approximately 3–4 times as many experiments in the same time period as with standard effluent sampling and analysis. However, the method is not useful for decaying chemical species unless the exact decay rate constant is known in advance since the concentration curve at early times must be scaled to the known injected mass. Also, because fluorescence is measured, the method is limited to fluorescent solute tracers and fluorescent polystyrene microspheres (colloidal suspensions).

References

Anders, R., Chrysikopoulos, C.V., 2005. Virus fate and transport during artificial recharge with recycled water. Water Resources Research 41 (10), W10415, doi:10.1029/2004WR003419.

Anders, R., Chrysikopoulos, C.V., 2009. Transport of viruses through saturated and unsaturated columns packed with sand. Transport in Porous Media 76, 121–138, doi:10.1007/s11242-008-9239-3.

Barg, S., Koch, D., Pulkin, M., Grathwohl, G., 2008. Modeling of glass sintering applied for the fabrication of porous glass bodies. Journal of Materials Science 43, 483–488, doi:10.1007/s10853-007-1873-6.

Baumann, T., Werth, C.J., 2004. Visualization and modeling of polystyrol colloid transport in a silicon micromodel. Vadose Zone Journal 3, 434–443.

Beresnev, I.A., Vigil, R., Li, W., Pennington, W.D., Turpening, R.M., Iassonov, P.P., Ewing, R.P., 2005. Elastic waves push organic fluids from reservoir rock. Geophysical Research Letters 32, L13303, doi:10.1029/2005GL023123.

Bouhairie, S., 1998. A study of the entrapment process in a recirculation flow by video-imaging method. M.S. Thesis, McGill University, Montreal, Canada.

Bradford, S.A., Bettahar, M., Simunek, J., van Genuchten, M.Th., 2004. Straining and attachment of colloids in physically heterogeneous porous media. Vadose Zone Journal 3, 384–394.

Chrysikopoulos, C.V., 1993. Artificial tracers for geothermal reservoir studies. Environmental Geology 22, 60–70.
Chrysikopoulos, C.V., Vogler, E.T., 2004. Acoustically enhanced multicomponent NAPL ganglia dissolution in water saturated packed columns. Environmental Science and Technology 38 (10), 2940–2945.
Chrysikopoulos, C.V., Masciopinto, C., La Mantia, R., Manariotis, I.D., 2010. Removal of biocolloids suspended in reclaimed wastewater by injection in a fractured aquifer model. Environmental Science and Technology 44 (3), 971–977.
Dai, Z., Samper, J., 2004. Inverse problem of multicomponent reactive chemical transport in porous media: formulation and applications. Water Resources Research 40, W07407, doi:10.1029/2004WR003248.
Darcy, H., 1856. Les Fontaines Publiques de la Ville de Dijon. V. Dalmont, Paris 647 pp.
DeNovio, N.M., Saiers, J.E., Ryan, J.N., 2004. Colloid movement in unsaturated porous media: recent advances and future directions. Vadose Zone Journal 3, 338–351.
Gomis-Yagües, V., Boluda-Botella, N., Ruiz-Beviá, F., 1997. Column displacement experiments to validate hydrogeochemical models of seawater intrusions. Journal of Contaminant Hydrology 29, 81–91.
Gross, A., Besov, A., Reck, D.D., Sorek, S., Ben-Dor, G., Britan, A., Palchikov, E., 2003. Application of waves for remediation of contaminated aquifers. Environmental Science and Technology 37, 4481–4486.
Harmon, T.C., Kim, T.J., Dela Barre, B.K., Chrysikopoulos, C.V., 1999. Modeling cosolvent–water displacement in porous media using a variable density and viscosity flow and transport approach. Journal of Environmental Engineering (ASCE) 125 (1), 87–91.
Harter, T., Wagner, S., Atwill, E.R., 2000. Colloid transport and filtration of *Cryptosporidium parvum* in sandy soils and aquifer sediments. Environmental Science and Technology 34, 62–70.
Jin, Y., Chu, Y., Li, Y., 2000. Virus removal and transport in saturated and unsaturated sand columns. Journal of Contaminant Hydrology 43, 111–128.
Keller, A.A., Sirivithayapakorn, S., Chrysikopoulos, C.V., 2004. Early breakthrough of colloids and bacteriophage MS2 in a water-saturated sand column. Water Resources Research 40 (8), W08304, doi:10.1029/2003WR002676.
Kreft, A., Zuber, A., 1986. Comments on "flux-averaged and volume-averaged concentrations in continuum approaches to solute transport" by J.C. Parker and M.Th. van Genuchten. Water Resources Research 22 (7), 1157–1158.
Kumar, T.S., Patle, M.K., Sujith, R.I., 2007. Characteristics of acoustic standing waves in packed-bed columns. AIChE Journal 53 (2), 297–304.
Li, W., Vigil, R.D., Beresnev, I.A., Iassonov, P., Ewing, R., 2005. Vibration-induced mobilization of trapped oil ganglia in porous media: experimental validation of capillary-physics mechanism. Journal of Colloid and Interface Science 289, 193–199.
Li, Y., Wang, Y., Pennell, K.D., Abriola, L.M., 2008. Investigation of the transport and deposition of fullerene (C60) nanoparticles in quartz sand under varying flow conditions. Environmental Science and Technology 42, 7174–7180, doi:10.1021/es801305y.
Liu, W., Lo, J., Tsai, C., 1992. On-line method for measurement of the dispersion coefficient of radionuclide migration using a column method. Journal of Radioanalytical and Nuclear Chemistry 163 (2), 373–384.
MathWorks, Inc., 2008. Image Processing Toolbox™ User's Guide, Natick, MA.
Masciopinto, C., La Mantia, R., Chrysikopoulos, C.V., 2008. Fate and transport of pathogens in a fractured aquifer in the Salento area, Italy. Water Resources Research 44, W01404, doi:10.1029/2006WR005643.
Northrup, M.A., Kulp, T.J., Angel, S.M., Pinder, G.F., 1993. Direct measurement of interstitial velocity field variations in a porous medium using fluorescent-particle image velocimetry. Chemical Engineering Science 48 (1), 13–21.
Olson, M.S., Ford, R.M., Smith, J.A., Fernandez, E.J., 2004. Quantification of bacterial chemotaxis in porous media using magnetic resonance imaging. Environmental Science and Technology 38 (14), 3864–3870.
Parker, J.C., van Genuchten, M.Th., 1984. Flux-averaged and volume-averaged concentrations in continuum approaches to solute transport. Water Resources Research 20 (7), 866–872.
Peurrung, L.M., Rashidi, M., Kulp, T.J., 1995. Measurement of porous medium velocity fields and their volumetric averaging characteristics using particle tracking velocimetry. Chemical Engineering Science 50 (14), 2243–2253.
Plona, T.J., 1980. Observation of a second bulk compressional wave in a porous medium at ultrasonic frequencies. Applied Physics Letters 36 (4), 259–261, doi:10.1063/1.91445.
Prado, M.O., Fredericci, C., Zanotto, E.D., 2003. Isothermal sintering with concurrent crystallization of polydispersed soda-lime-silica glass beads. Journal of Non-Crystalline Solids 331, 145–156, doi:10.1016/j.jnoncrysol.2003.08.076.
Rashidi, M., Peurrung, L., Tompson, A.F.B., Kulp, T.J., 1996. Experimental analysis of pore-scale flow and transport in porous media. Advances in Water Resources 19 (3), 163–180.
Roberts, P.M., 2005. Laboratory observations of altered porous fluid flow behavior in Brea sandstone induced by low-frequency dynamic stress stimulation. Acoustical Physics 51 (s1), s140–s148.
Roberts, P.M., Sharma, A., Uddameri, V., Monagle, M., Dale, D.E., Steck, L.K., 2001. Enhanced DNAPL transport in a sand core during dynamic stress stimulation. Environmental Engineering Science 18 (2), 67–79.
Rockhold, M.L., Yarwood, R.R., Niemet, M.R., Bottomley, P.J., Selker, J.S., 2005. Experimental observations and numerical modeling of coupled microbial and transport processes in variably saturated sand. Vadose Zone Journal 4, 407–417, doi:10.2136/vzj2004.0087.
Shang, J., Flury, M., Chen, G., Zhuang, J., 2008. Impact of flow rate, water content, and capillary forces on in situ colloid mobilization during infiltration in unsaturated sediments. Water Resources Research 44 (1–12), W06411, doi:10.1029/2007WR006516.
Sherwood, J.L., Sung, J.C., Ford, R.M., Fernandez, E.J., Maneval, J.E., Smith, J.A., 2003. Analysis of bacterial random motility in a porous medium using magnetic resonance imaging and immunomagnetic labeling. Environmental Science and Technology 37 (4), 781–785.
Thomas, J.M., Chrysikopoulos, C.V., 2007. Experimental investigation of acoustically enhanced colloid transport in water-saturated packed columns. Journal of Colloid and Interface Science 308, 200–207, doi:10.1016/j.jcis.2006.12.062.
Tufenkji, N., 2007. Modeling microbial transport in porous media: traditional approaches and recent developments. Advances in Water Resources 30, 1455–1469.
Vogler, E.T., Chrysikopoulos, C.V., 2002. Experimental investigation of acoustically enhanced solute transport in porous media. Geophysical Research Letters 29 (15), 1–4, doi:10.1029/2002GL015304.
Vogler, E.T., Chrysikopoulos, C.V., 2004. An experimental study of acoustically enhanced NAPL dissolution in porous media. AIChE Journal 50 (12), 3271–3280, doi:10.1002/aic.10221.
Wang, M., Ford, R.M., 2009. Transverse bacterial migration induced by chemotaxis in a column with structured physical heterogeneity. Environmental Science and Technology 43 (15), 5921–5927.
Yoon, J.S., Germaine, J.T., Culligan, P.J., 2006. Visualization of particle behavior within a porous medium: mechanisms for particle filtration and retardation. Water Resources Research 42 (1–16), W06417, doi:10.1029/2004WR003660.
Zhang, W., 2003. Nanoscale iron particles for environmental remediation: an overview. Journal of Nanoparticle Research 5, 323–332.
Zhuang, J., Jin, Y., 2003. Virus retention and transport through Al-oxide coated sand columns: effects of ionic strength and composition. Journal of Contaminant Hydrology 60, 193–209.